wind

MDPI

Article

Analysis of the Skyscraper Wind around High-Rise Buildings in Coastal Region, South Korea, during Typhoon 'Hinnamnor'

Jongyeong Kim, Yongju Kwon, Byeonggug Kang, Joowon Choi and Soonchul Kwon *

Department of Civil & Environmental Engineering, Pusan National University, Busan 46241, Republic of Korea
* Correspondence: sckwon@pusan.ac.kr; Tel.: +82-51-510-7640

Abstract: High-rise buildings in cities adversely affect wind regimes by changing the air currents in their surrounding areas. In particular, extreme climate phenomena caused by climate change are stronger and more frequent, causing damage in cities. To better understand skyscraper wind behaviors around high-rise buildings, actual measurements are necessary to determine the environmental assessment of the wind effect. In this study, field measurements were performed with five anemometers at five points in the vicinity of a skyscraper called the LCT residential complex (411.6 m tall) surrounded by high-rise buildings in the coastal city of Busan, South Korea during Typhoon Hinnamnor. The gust was 3.7 times stronger, while the maximum 1-min mean wind speed was 3.1 times stronger than those measured at a nearby reference weather station operated by the Korean Meteorological Administration. The characteristics of downward and canyon winds were shown to depend on the spatiotemporal characteristics of the five points. The turbulence intensity declined as the wind speed increased and converged to a certain value. The gust factor also dropped as the wind speed increased and converged to 2.0, and was considered to be the parameter that best represents the intensity of instantaneous gust caused by the skyscraper wind effect. These results suggest that high-rise buildings should be designed with the consideration of gusts twice as strong as the average wind speed. In addition, field measurements should be accompanied in order to respond to the skyscraper wind effect.

Keywords: field measurement; typhoon; high-rise buildings; strong winds

Citation: Kim, J.; Kwon, Y.; Kang, B.; Choi, J.; Kwon, S. Analysis of the Skyscraper Wind around High-Rise Buildings in Coastal Region, South Korea, during Typhoon 'Hinnamnor'. *Wind* **2023**, *3*, 64–78. https://doi.org/10.3390/wind3010005

Academic Editor: Charalampos Baniotopoulos

Received: 2 December 2022
Revised: 5 February 2023
Accepted: 7 February 2023
Published: 13 February 2023

1. Introduction

In recent years, many cities worldwide, particularly those with high-rise buildings, have been increasingly affected by strong winds. Though indicative of economic wealth, high-rise buildings in cities also exert adverse impacts on the safety, living environment quality, and socio-economic well-being of urban populations [1–4]. For example, wind strikes high-rise buildings, creating strong winds and eddies around buildings, called skyscraper wind. The skyscraper wind effect grows stronger with extreme weather events such as typhoons, which have intensified under global climate change. Skyscraper wind generates gusts that threaten the safety of pedestrians and buildings due to flying debris. Therefore, skyscraper wind has been considered as a new issue in cities. Although a social and environmental awareness of skyscraper wind is still lacking in South Korea despite a recent overcrowding of high-rise buildings, many countries such as the United States, United Kingdom, Canada, the Netherlands, and Japan have issued standards for multi-dimensional impact assessments [5–9]. Many studies have been carried out to analyze and predict the characteristics of skyscraper wind as well as to determine its effects on society. For example, Razak et al., performed large-eddy simulations (LES) of airflows around various types of block arrays to estimate the pedestrian wind environment [10]. Kwon et al., performed computational fluid dynamic (CFD) simulations by employing user defined functions (UDFs) to reconstruct the real wind environment under extreme weather events [11]. By using CFD simulations, Kheyari and Dalui quantified interference effects

depending on the various shapes and sizes of a building and its surrounding interference and orientation [12]. Similarly, Mou et al., simulated the wind pressure distributions around squared-shaped tall buildings [13]. Based on CFD simulations, Zheng et al., modeled the influences of surrounding buildings with different heights, densities, and arrangements on the target building [14]. On the other hand, studies such as wind effect monitoring in high-rise buildings, wind tunnel experiments, and a comparison of the two methods are also being conducted [15–17]. In the literature, few studies have analyzed the skyscraper wind effects in response to the different shapes and arrangements of buildings via LES and CFD simulations. Uncertainties associated with unstable turbulences and low accuracy of boundary conditions, in particular, under extreme weather conditions such as typhoons, may significantly reduce the accuracy and precision of LES and CFD simulations to reconstruct the actual wind environment. Thus, continuous field measurements to represent actual weather and geographic information are needed to quantify and predict the influence of skyscraper wind generated by high-rise buildings. In this study, we carried out field measurements with five anemometers at the LCT residential complex in the coastal urban area in Busan, South Korea and analyzed the monitoring of gust factors and the turbulence intensity dependent on wind speed, which represents the intensity of the instantaneous gust caused by the skyscraper wind effect.

2. Materials and Methods

2.1. Research Period

Figure 1 shows the path of Hinnamnor, the eleventh typhoon in 2022. It developed into a typhoon in the southern sea of Japan on 28 August, and when it landed on Jeju Island on the evening of 5 September, the central pressure was 940 hpa, the lowest central pressure measured by the Korean Meteorological Administration (KMA). The center of the typhoon passed right through the study area. When approaching the research site, the central pressure was maintained at 950 hpa and the maximum instantaneous wind speed was approximately 40 m/s. It then escaped to the East Sea and disappeared at 21:00, 6 September. Therefore, in this study, we analyzed the data for 48 h from 00:00 on 5 September 2022 to 00:00 on 7 September 2022 when the research site was affected by the typhoon.

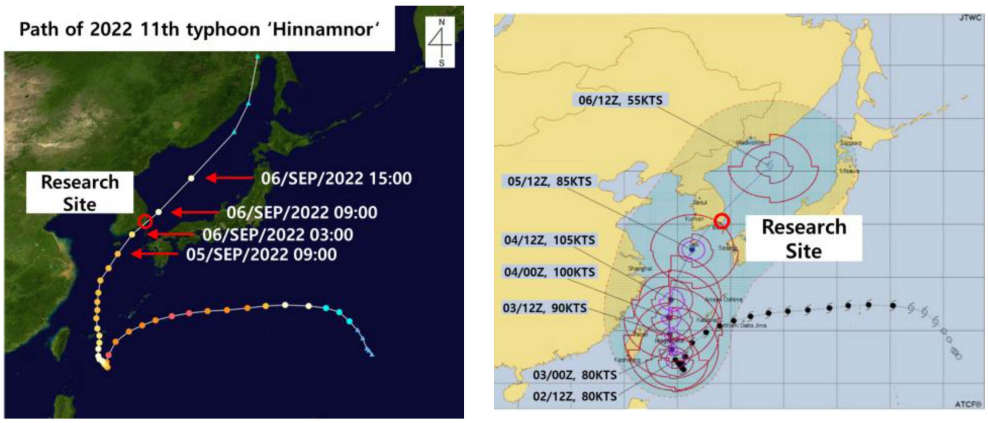

Figure 1. Spatiotemporal path of Typhoon Hinnamnor in relation to the study site (JTWC).

2.2. Research Site

The research site was selected as the vicinity of the LCT residential complex, located in Haeundae-gu, Busan, a coastal city in South Korea (Figure 2). To observe the skyscraper wind, it was necessary to measure the wind speed and direction affected by the concentrated high-rise buildings. The LCT residential complex consists of three buildings: Landmark Tower, A Tower, and B Tower. In the area around the LCT are buildings with a significantly lower height, where local strong winds or scattered winds blow. Since LCT is located in a coastal area that is vulnerable to storm and flood damage, its skyscraper winds frequently

damage the surrounding areas. LCT Landmark Tower is currently the second tallest building in Korea with a height of 411.6 m (Figure 2). Since the construction of the LCT residential complex, adverse effects such as damaged buildings, flying debris, and noise have continuously occurred in its neighboring areas.

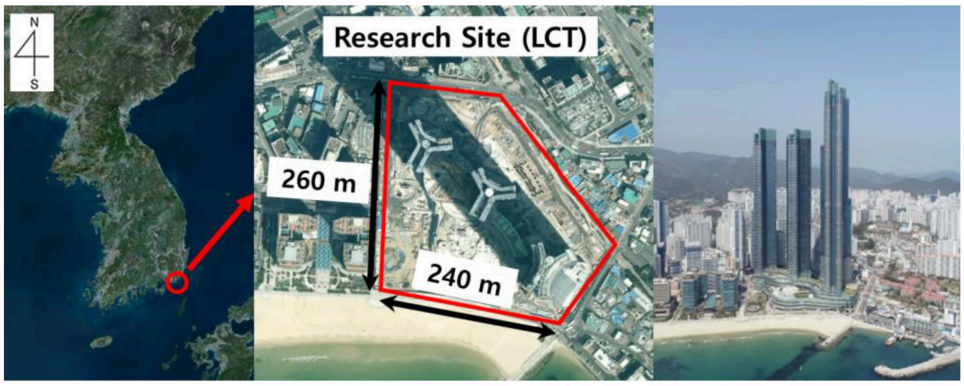

Figure 2. Geographical location and surrounding area of the LCT residential complex (self-taken).

2.3. Main Observation Points

Before installing anemometers to investigate the skyscraper wind enhanced by the typhoon, we investigated the vicinity of the LCT residential complex in order to design a sampling strategy to best measure and infer the wind characteristics. We concluded that roadsides were necessary points to observe the effect of the skyscraper wind because, as the wind passes between the buildings and the road corners, the wind direction and speed change from one road to another. In addition, we selected the main and secondary entrances for pedestrians using the residential and commercial complex as observation points. The locations of the main observation points are shown in Figure 3.

Figure 3. Field measurement points (1~20) around the LCT residential complex.

Out of the 20 field measurement points, we selected five points to install the anemometers. The points were selected as the points where strong winds flow from the open sea (L-1, L-5), the points where the strong wind speed was measured (L-1, L-2, and L-3), and where the intersection occurred (L-2, L-3, L-4) (Figure 4).

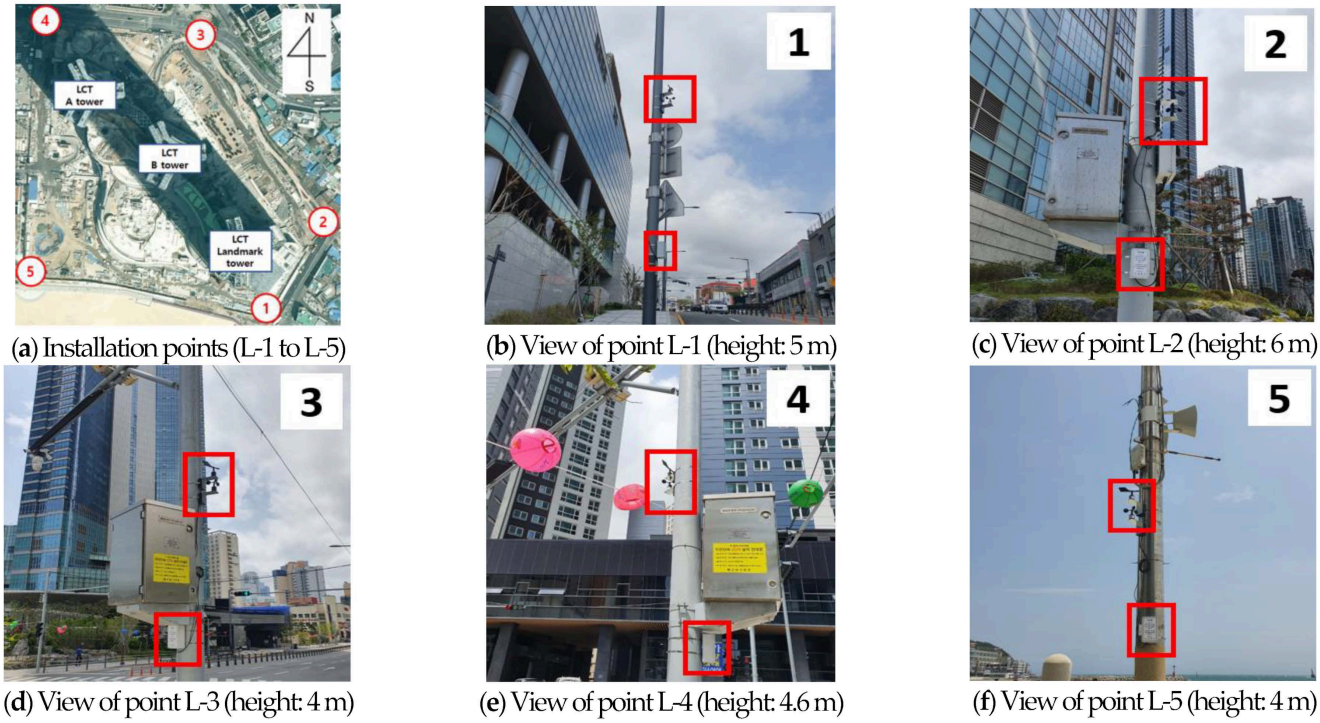

(**a**) Installation points (L-1 to L-5) (**b**) View of point L-1 (height: 5 m) (**c**) View of point L-2 (height: 6 m)

(**d**) View of point L-3 (height: 4 m) (**e**) View of point L-4 (height: 4.6 m) (**f**) View of point L-5 (height: 4 m)

Figure 4. Field measurement points (1~5) around the LCT residential complex. (**a**) Locations of the installation points. (**b**–**f**) Views of points L-1 to L-5, respectively.

2.4. Monitoring Anemometers

Five anemometers were installed at a height of 4.0 to 8.0 m in consideration of the field conditions (Figure 4). In general, the measuring equipment should be more than 1 m away from the mast to minimize disturbance, but local governments suggest installing supporters as short as possible to prevent damage caused by strong winds. We utilized the anemometers (ARCO-SERIAL model) (Figure 5) according to the 'Standard Specification for Automatic Meteorological Observation Equipment' of the KMA [18]. Their related specifications are shown in Table 1. L-1, L-2, and L-4, located on the side of the LCT residential complex, were expected to be affected by downward winds and separated winds. L-3 was expected to be affected by canyon winds when southerly winds blew and separated winds from the Landmark Tower and B Tower when southeast winds blew. L-5 was expected to receive the uninterrupted sea breeze and the canyon winds blowing from the northeast.

Table 1. Specifications of the anemometers.

	Wind Speed	**Wind Direction**
Range	0~70 m/s	0~360°
Accuracy	±2%	±1°
Resolution	0.1 m/s	1°

The anemometer recorded four data readings per second [18]. The last 240 data readings collected for one minute were averaged to calculate the 1-min mean wind directions and wind speeds.

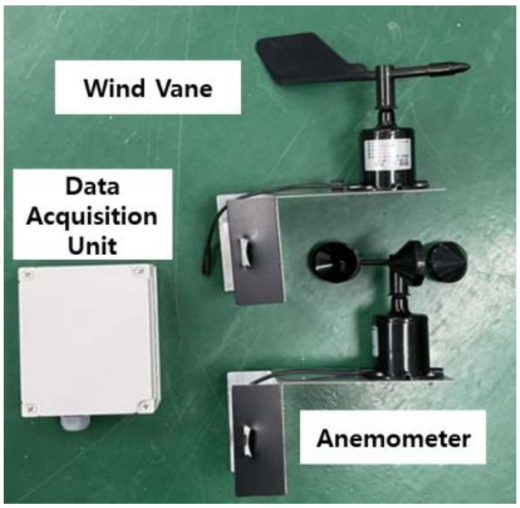

Figure 5. Anemometer configuration.

2.5. Haeundae Meteorological Observatory

The Haeundae Meteorological Observatory Auto Weathering System (AWS) in Haeundae, operated by KMA, is located 1.8 km northwest of the research site (Figure 6). The nearest reference station (AWS) was selected as a control point to compare and analyze the effects of the skyscraper wind. The LCT residential complex is directly exposed to the sea breeze, whereas AWS is located relatively inland, suggesting that the wind speed is expected to be relatively low.

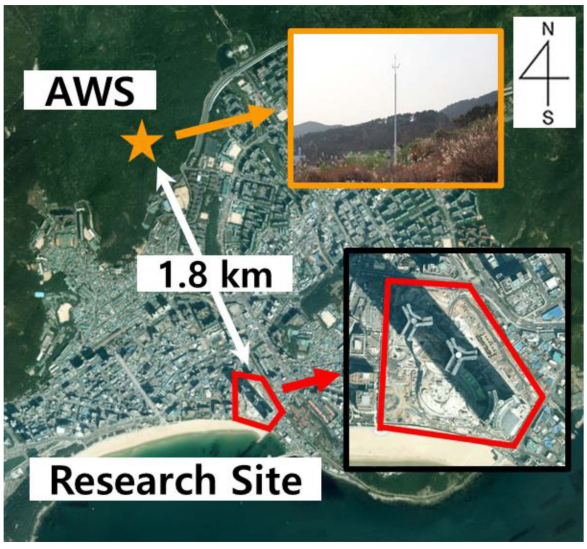

Figure 6. Locations of the study site and AWS.

AWS provides the 1-min mean data of wind speed and wind direction with the shortest period of time series data and the daily maximum gust as the statistical data. Using the data for the research period, we presented the windrose diagram with the 1-min mean data in Figure 7. The main wind directions were north–northeast (38%) and northeast (24%), while the max 1-min mean wind speed was 12.3 m/s (NNE), lower than the maximum wind speed of the typhoon.

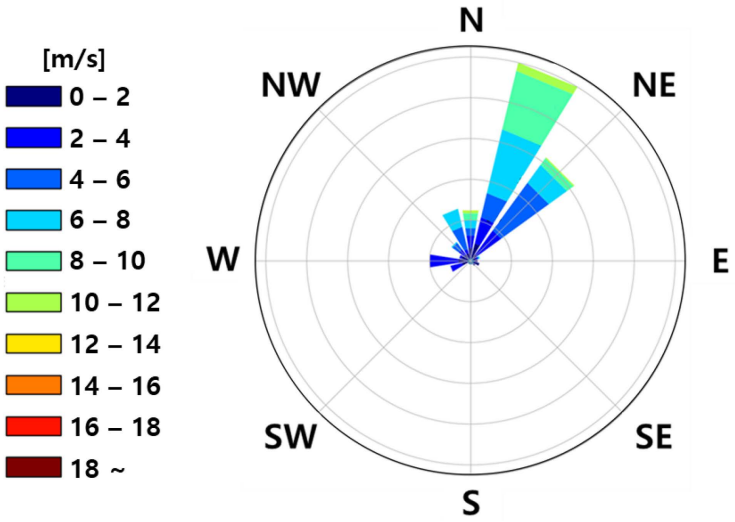

Figure 7. Windrose at AWS.

3. Results

Based on a comparison of wind speed from AWS and those from the anemometers, we estimated the rate of increase in the wind speed for the area adjacent to the LCT residential complex, and quantified the fluctuation of the skyscraper wind by introducing the Beaufort wind scale, turbulence intensity, and gust factor.

3.1. Mean and Maximum Wind Speeds and Directions

Figure 8 shows a time series comparison of the 1-min average wind speed (U) at AWS (□), the reference station, and at the five points (●) (L-1 to L-5). In addition, the wind speed and wind direction when the wind speed was the highest at each point are shown in more detail. The statistical distribution of wind at each point was visualized using the windrose diagram in Figure 9. Data were averaged after the missing data, outliers, and data exceeding the measurable wind speed range (>70 m/s) were removed. As the center of the typhoon passed through the research site, the data show the characteristics of a steep descent after reaching the peak wind speed. Table 2 shows the wind speed and wind direction for the max peak gusts, the max 1-min mean wind speeds, and the max 10-min mean wind speeds (the most frequently used) at each point. The relatively strong winds were observed at L-1, L-2, and L-3.

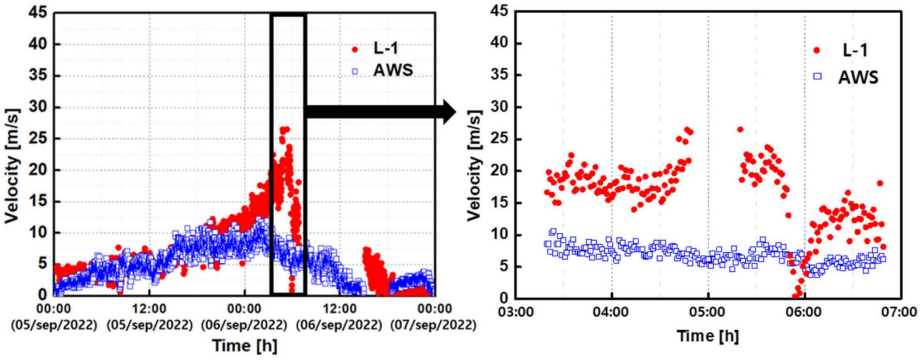

(**a**) Wind speed comparison (L-1 ● vs. AWS □)

Figure 8. *Cont.*

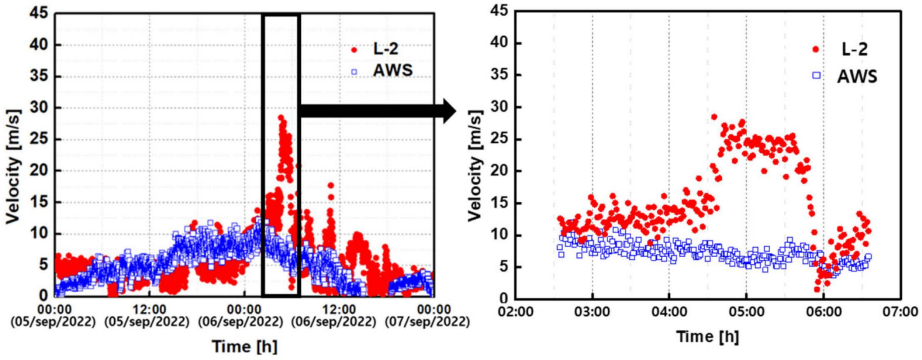

(**b**) Wind speed comparison (L-2 ● vs. AWS □)

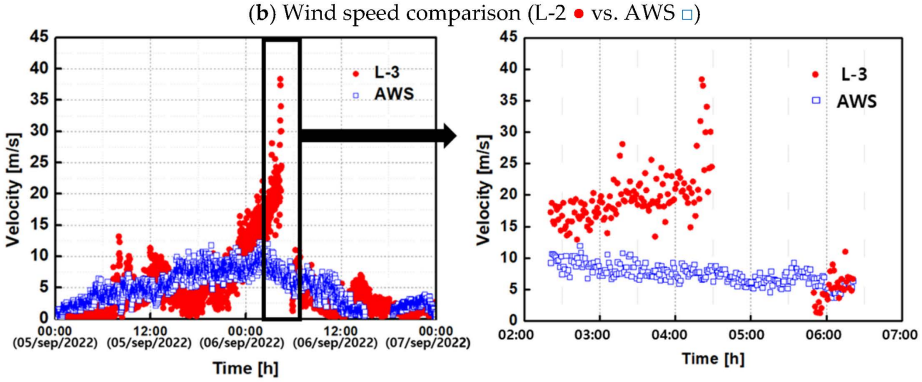

(**c**) Wind speed comparison (L-3 ● vs. AWS □)

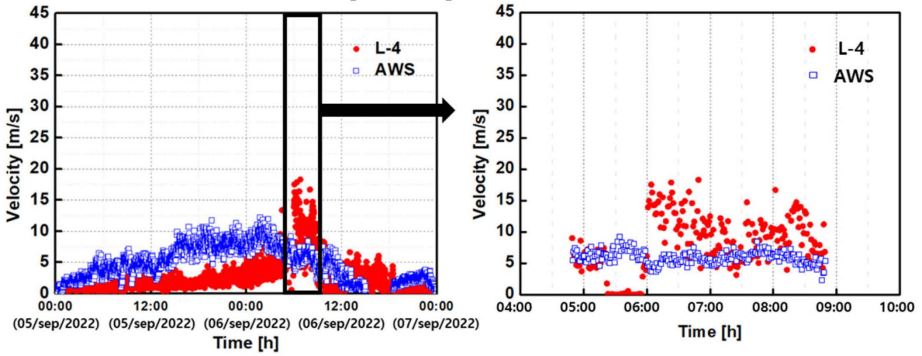

(**d**) Wind speed comparison (L-4 ● vs. AWS □)

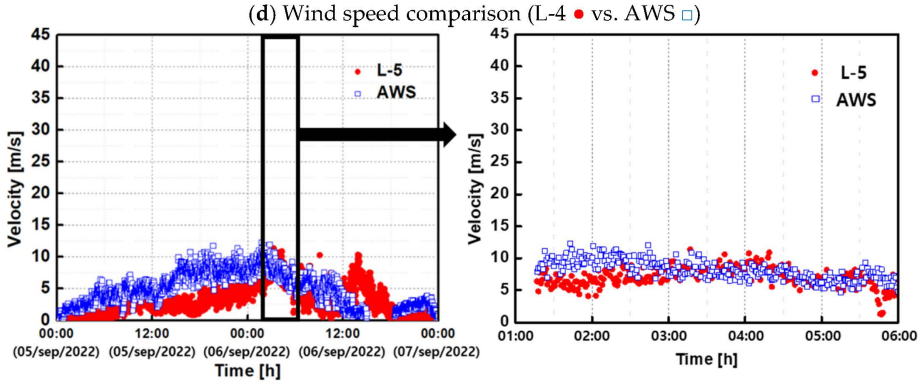

(**e**) Wind speed comparison (L-5 ● vs. AWS □)

Figure 8. Comparison of the 1-min mean wind speeds over time (LCT residential complex vs. AWS) for (**a**–**e**) L-1 to L-5 (●) vs. AWS (□).

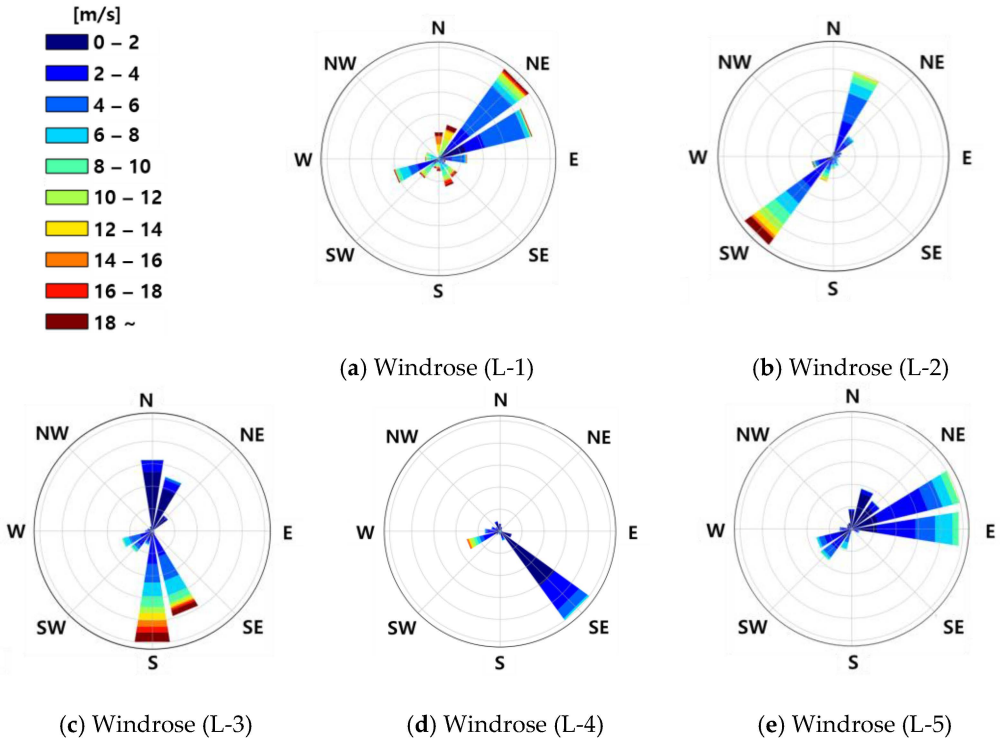

(**a**) Windrose (L-1) (**b**) Windrose (L-2)

(**c**) Windrose (L-3) (**d**) Windrose (L-4) (**e**) Windrose (L-5)

Figure 9. Windrose at each point (**a**–**e**) L-1 to L-5, respectively.

Table 2. The mean wind speeds and peak gusts at each point (L-1 to L-5 and AWS).

Point	Max Peak Gust (m/s)	Wind Direction		Max 1 min-Mean Wind Speed (m/s)	Wind Direction		Max 10 min-Mean Wind Speed (m/s)	Wind Direction	
L-1	44.19	10.1°	N	26.52	10.0°	N	22.57	33.3°	NNE
L-2	40.80	226.3°	SW	28.48	228.3°	SW	25.05	233.1°	SW
L-3	55.53	147.8°	SSE	38.39	147.2°	SSE	29.49	152.3°	SSE
L-4	45.68	238.8°	WSW	18.31	235.3°	SW	13.75	238.9°	WSW
L-5	21.03	56.0°	NE	11.35	74.7°	ENE	9.1	212.8°	SSW
AWS	15.20	81.6°	E	12.30	7.7°	N	10.11	10.5°	N

L-1 was installed at the eastern corner of the LCT residential complex, with its wind direction concentrated in the northeast (24%), east–northeast (21%), and west–southwest (10%). Due to the spatiotemporal characteristics of L-1, this pattern appeared to be caused by separated winds that blew parallel to the side of the LCT residential complex (Figure 10). The max peak gust and max 1-min mean wind speed were 26.52 m/s (N) and 44.19 m/s (N), respectively, which were 2.9 times and 2.2 times stronger than the wind speed at AWS, respectively.

Due to the same spatiotemporal characteristics as L-1, L-2 was concentrated in a specific wind direction by the separated wind, which led to a stronger wind speed in the main direction (Figures 9 and 10). The max peak gust and max 1-min mean wind speed at L-2 were 40.80 m/s (SW) and 28.48 m/s (SW), respectively, which were 2.7 and 2.3 times stronger than the wind speed of AWS, respectively.

L-3 was installed at the intersection on the north side of the LCT residential complex. The canyon wind passing between the three buildings located in the south showed that the southerly wind was significantly stronger than the northerly wind, with a significant effect on the increase in wind speed (Figures 9 and 11). At this point, the strongest wind

was observed in this typhoon event, and the max peak gust and max 1-min mean wind speed were 55.53 m/s (SSE) and 38.39 m/s (SSE), respectively, which were 3.7 and 3.1 times stronger than the wind speed at AWS, respectively.

Figure 10. Main wind direction for L-1 (**left**) and L-2 (**right**).

Figure 11. Main wind direction for L-3 (**left**) and L-4 (**right**).

On the other hand, lower wind speeds were observed at L-4 and L-5 than at L-1, L-2, and L-3. The main wind direction at L-4 was southeast. The reduction in the wind speed was attributed to the effects of trees located on the windward side of the area, where the skyscraper winds were expected. After the center of the typhoon passed, strong winds were observed from the southwest winds blowing along the narrow road. Since L-5, in the southern part of the LCT residential complex, was located on the opposite side of L-3, strong northerly winds were expected. However, the lowest wind speed was observed at L-5, similar to that of AWS, which was not affected by skyscraper wind. In Toronto, Canada, a set-back structure shape is recommended to reduce skyscraper winds caused by high-rise buildings [19]. On the south side of the LCT residential complex, buildings have a set-back shape(Figure 12), thus the skyscraper wind is alleviated. This, in turn, warrants an in-depth study on the set-back structure shape that mitigates the skyscraper wind.

3.2. Beaufort Wind Scale

In Section 3.1., we analyzed the relative strength of the wind speed based on the comparison of the wind speeds at the five points with that observed at AWS. Here, we also analyzed the strength of the wind speed in absolute values through the Beaufort Wind Scale, devised by the World Meteorological Organization (WMO) in Table 3. The strength of the wind speed is divided into 13 grades and shown in Figure 13.

At AWS, winds of grades 0–6 blew. The most frequent wind speed grade was a moderate breeze (grade 4) (27.09%), while the maximum wind speed was a strong breeze (grade 6) (0.82%). At L-1, L-2, and L-3, grades 10 (storm), 10 (storm), and 12 (hurricane) appeared, respectively. The range of grade 10 or higher was strong enough to be described as 'uprooting trees and causing great damage to buildings'. At L-1, L-2, and L-3, the wind speed frequency was above grade 6 (10.8 m/s), higher than that at AWS. The frequency of

the wind speed in the range of grades 4 and 5 (5.5~10.8 m/s) was higher at AWS than that at the five points. In other words, the skyscraper wind grew more pronounced when the mass flux rose above a certain wind speed. At L-4, the maximum wind speed grade was grade 8 (gale, 0.1%) while the most frequent wind speed grade was 1 (light air). This, in turn, indicates that the overall wind speed was low while strong winds blew temporarily. L-5 generally showed a low Beaufort number.

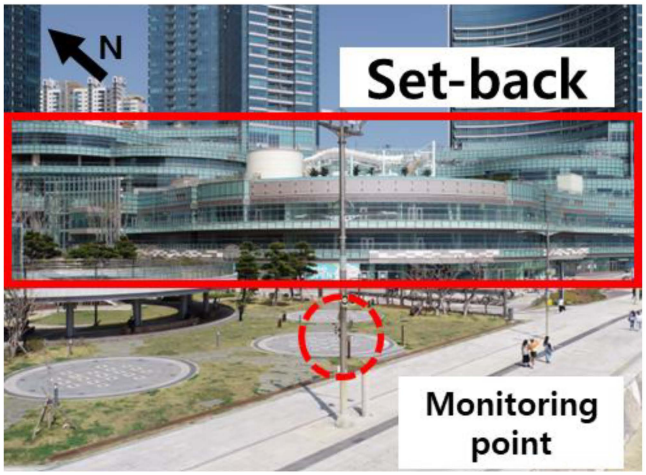

Figure 12. Buildings with a set-back structure shape on the south side of the LCT residential complex.

Table 3. Beaufort Wind Scale.

Beaufort Number	Description	Wind Speed (m/s)
0	Calm	0~0.2
1	Light air	0.3~1.5
2	Light breeze	1.6~3.3
3	Gentle breeze	3.4~5.4
4	Moderate breeze	5.5~7.9
5	Fresh breeze	8.0~10.7
6	Strong breeze	10.8~13.8
7	Near gale	13.9~17.1
8	Gale	17.2~20.7
9	Severe gale	20.8~24.4
10	Storm	24.5~28.4
11	Violent storm	28.5~32.6
12	Hurricane	32.7~

3.3. Turbulence Intensity

We also analyzed the wind fluctuation characteristics observed at the five points. Overall, the wind showed a spatiotemporally irregular distribution. In the atmospheric boundary layer, the air does not flow uniformly due to the roughness of the ground surface or the frictional effect of structures, and fluctuation characteristics such as the formation of vortices increase. In particular, as the study site was a single high-rise building surrounded by low-rise buildings, the airflow was very unstable [20]. Turbulence intensity (I), which represents the wind fluctuation characteristics, is defined as the ratio of the standard deviation (σ) of the wind speed to the mean wind speed (U) as follows:

$$I = \frac{\sigma}{U}$$
$$\sigma = \sqrt{\frac{1}{T}\int_{t_0-T}^{t_0} u^2(t)dt}$$

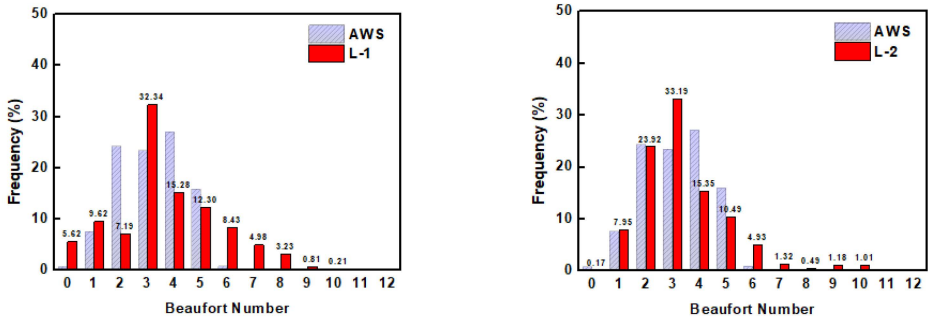

(**a**) Beaufort number comparison (L-1 ■ vs. AWS ■)

(**b**) Beaufort number comparison (L-2 ● vs. AWS ■)

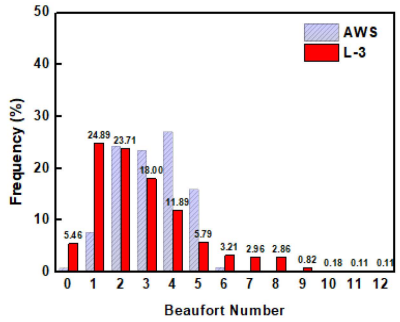

(**c**) Beaufort number comparison (L-3 ■ vs. AWS ■)

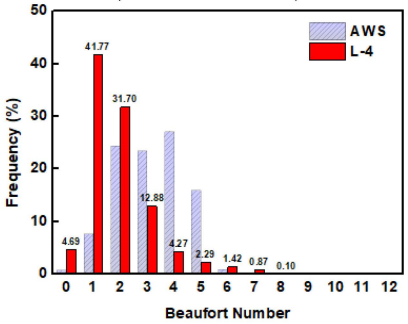

(**d**) Beaufort number comparison (L-4 ■ vs. AWS ■)

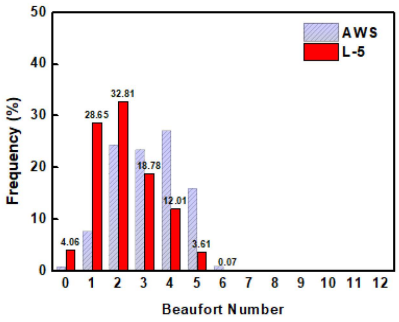

(**e**) Beaufort Number comparison (L-4 ■ vs. AWS ■)

Figure 13. Frequency of the Beaufort numbers at each point for LCT (**a**–**e**) L-1 to L-5 (■), respectively, vs. AWS (■).

Figure 14 shows the relationship between the mean wind speed and turbulence intensity at each point. In line with previous studies, the turbulence intensity fell as the mean wind speed rose, and converged above a certain wind speed [21,22].

When the wind speed was low, the frictional force acted more strongly than the inertial wind force, rendering the airflow unstable, and thus the turbulence intensity rose up to 0.95. However, when the wind speed was above 10 m/s, the range of turbulence intensity converged to 0.1–0.2 as the inertial wind force was increased by the high wind speed. Strong turbulence intensity, even at a high wind speed, was observed when the center of the typhoon, a windless zone, passed through the study site.

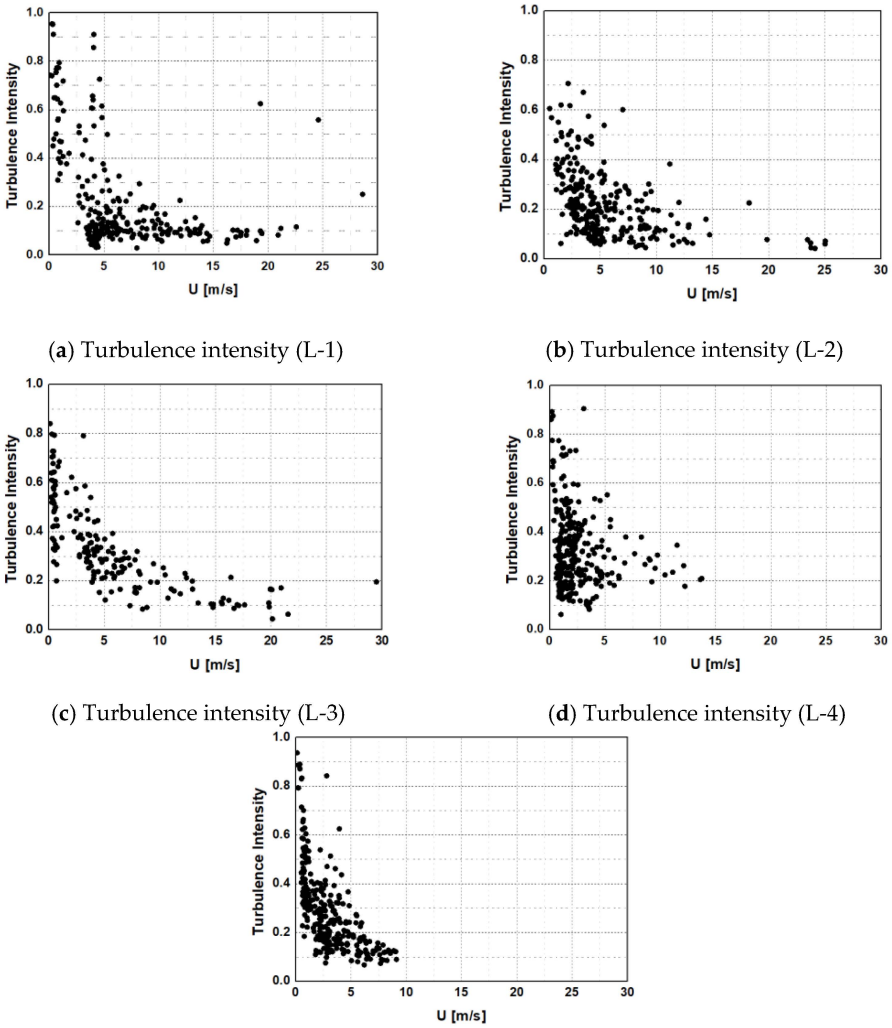

(**a**) Turbulence intensity (L-1)

(**b**) Turbulence intensity (L-2)

(**c**) Turbulence intensity (L-3)

(**d**) Turbulence intensity (L-4)

(**e**) Turbulence intensity (L-5)

Figure 14. Variations in the turbulence intensity with the mean speed for (**a**–**e**) L-1 to L-5, respectively.

3.4. Gust Factor

Exterior materials falling off buildings and structural damage to buildings are mainly caused by momentary gusts of winds, which can cause additional secondary damage and adversely affect the wind environment for pedestrians. The gust factor ($G_u = U_{max}/U$) is defined as the ratio of the maximum instantaneous wind speed (U_{max}) to the mean wind speed (U) as follows:

$$U_{max} = \frac{1}{T_0}\int_{t_0-\frac{T_0}{2}}^{t_0+\frac{T_0}{2}} U(t)dt$$

$$U = \frac{1}{T}\int_{t_0-\frac{T}{2}}^{t_0+\frac{T}{2}} U(t)dt$$

In general, a short interval of 1–5 s is used for the maximum instantaneous wind speed evaluation time (T_0), while an interval of 5–10 min is used for the average wind speed evaluation time (T). In this paper, we set T_0 to 3 s and T to 10 min. Since the maximum instantaneous wind speed varied depending on the topography, surrounding area structures (e.g., shape, type, and height), and wind speed, G_U may differ for each location. The American Society of Civil Engineers (ASCE) suggests a ratio of a 3-s mean wind speed to a 10-min mean wind speed of 1.43 as a conversion factor according to the measurement time of wind speed [23]. In addition, Ishizaki (1977) presented the results according to the evaluation time of the instantaneous wind speed at 10 m above the ground on flat land, as shown in Table 4 [24].

Table 4. The relationship between the evaluation time of the instantaneous wind speed and G_u.

Evaluation Time	1	5~10	30
G_u	1.5~1.7	1.3	1.2

Shuyang et al. (2009) evaluated G_u when Typhoon Maemi invaded Miyakojima, Japan and reported that it converged to 1.6 regardless of wind speed [25]. Although the overall wind speed was increased by the skyscraper wind effect, it was considered to be the parameter that best represented the characteristics of skyscraper wind, which causes damage by momentarily generating strong gusts.

In the research area, as the wind speed increased, G_u decreased and tended to converge to a certain value, in line with the trend of turbulence intensity (Figures 14 and 15). In the wind speed range higher than 5 m/s, G_u was found to converge to about 2.0 at all points. This in turn indicated that a gust at least twice as strong as the average wind speed was blowing. On the other hand, when the average wind speed was lower than 5 m/s, the gust factor had high volatility and appeared up to 9.17, but most of them were insignificant due to the low average wind speed.

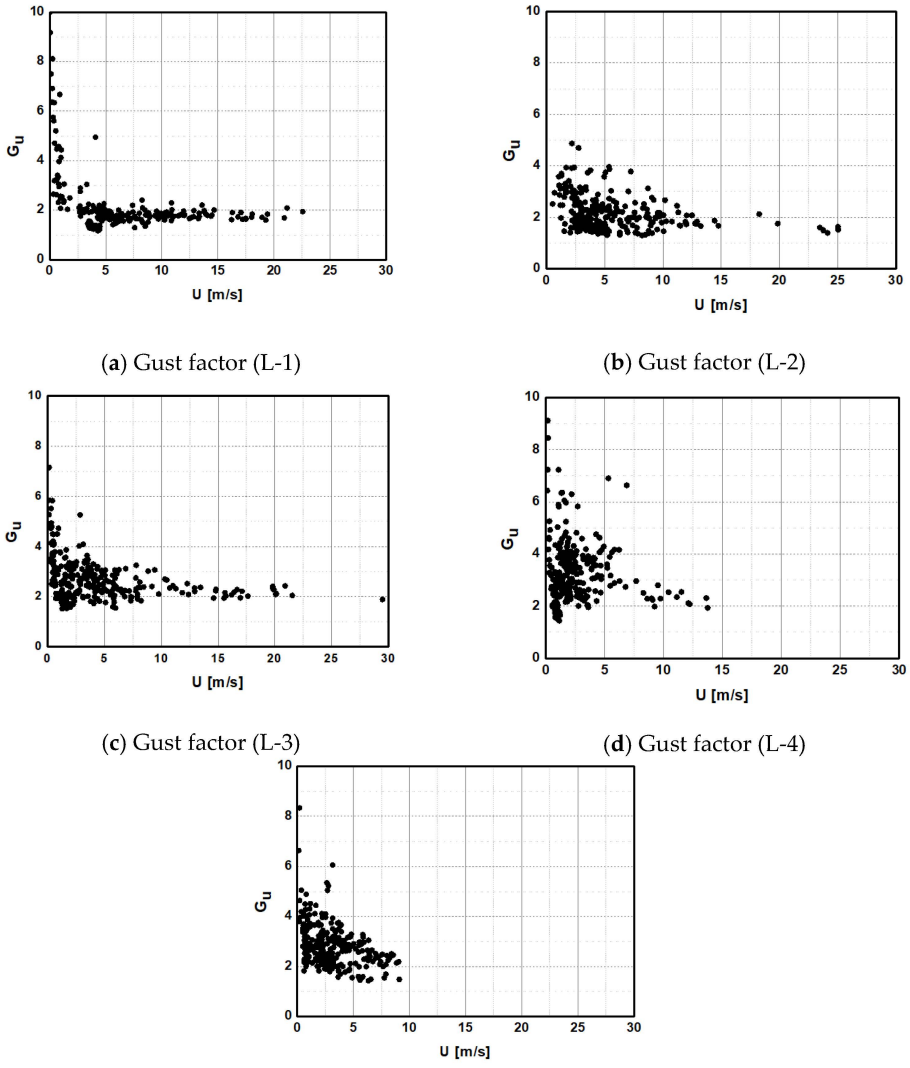

(**a**) Gust factor (L-1)

(**b**) Gust factor (L-2)

(**c**) Gust factor (L-3)

(**d**) Gust factor (L-4)

(**e**) Gust factor (L-5)

Figure 15. Variation in the gust factor with the mean wind speed. Values of the gust factor for (**a**) L-1, (**b**) L-2, (**c**) L-3, (**d**) L-4, and (**e**) L-5 are shown.

4. Summary and Conclusions

The study site was selected as the vicinity of the LCT residential complex. We measured the wind direction and speed via anemometers installed at five locations to determine the skyscraper wind behavior during Typhoon Hinnamnor. The skyscraper wind varied depending on the spatiotemporal characteristics of the study site such as complex interactions between the temperature, air pressure, building characteristics (e.g., arrangement and shape) in the vicinity, and landscaping. The gust and maximum 1-min mean wind speed were up to 3.7 and 3.1 times stronger than those measured at AWS, a nearby reference station, respectively. At AWS, the Beaufort number was up to 6, whereas the highest grade of 12 was observed in the vicinity of the LCT residential complex. This indicates that the wind speed was increased by the skyscraper wind effect. The turbulence intensity reached a maximum of 0.95 at low wind speed and declined as the wind speed increased, converging to a range of 0.1–0.2. Additionally, as the wind speed rose, the gust factor dropped. Regardless of the spatiotemporal characteristics of the five points, in the wind speed range higher than 5 m/s, it converged to about 2.0 at all points, resulting in a gust twice as strong as the mean wind speed at all points. These results suggest that when constructing high-rise buildings, it is necessary to consider that the gust is twice as strong as the average wind speed due to high fluctuation. In addition to mitigate the skyscraper wind effects, it would be helpful to plant trees or apply a set-back shape by predicting the wind conditions. Furthermore, this study provides actionable insights into accurate simulations of the drivers, patterns, and impacts of skyscraper wind and associated vulnerable areas under extreme weather conditions. In a future study, CFD simulations of spatiotemporally varying skyscraper wind effects and wind tunnel experiments for their validation will be performed.

Author Contributions: Conceptualization, S.K. and J.K.; methodology, J.K. and B.K.; validation, S.K. and J.K.; formal analysis, J.C. and B.K.; investigation, J.C. and Y.K.; resources, S.K.; data curation, J.K. and B.K.; writing—original draft preparation, J.K. and Y.K.; writing—review and editing, S.K.; visualization, Y.K.; supervision, S.K.; project administration, S.K. and J.K.; funding acquisition, S.K. All authors have read and agreed to the published version of the manuscript.

Funding: This research was supported by a grant (20011068) from the Regional Customized Disaster-Safety R&D Program funded by the Ministry of Interior and Safety (MOIS, Korea). This research was supported by the 2021 BK21 FOUR Program of Pusan National University.

Institutional Review Board Statement: Not applicable.

Informed Consent Statement: Not applicable.

Data Availability Statement: Not applicable.

Conflicts of Interest: The authors declare no conflict of interest.

References

1. Hwang, H.S.; Park, J.S. Research on Optimum Design Method for Fire Protection System of Super Tall Building. *Korean Inst. Fire Sci. Eng.* **2004**, *51*, 156.
2. Blocken, B.; Carmeliet, J. Pedestrian Wind Environment around Buildings: Literature Review and Practical Examples. *J. Build. Phys.* **2004**, *28*, 107–159. [CrossRef]
3. Blocken, B.; Stathpoulos, T.; Beeck, J.P.A.J. Pedestrian-level Wind Conditions around Buildings: Review of Wind-tunnel and CFD Techniques and Their Accuracy for Wind Comfort Assessment. *Build. Environ.* **2016**, *100*, 50–81. [CrossRef]
4. Mittal, H.; Sharma, A.; Gairola, A. A Review on the Study of Urban Wind at the Pedestrian Level around Buildings. *J. Build. Eng.* **2018**, *18*, 154–163. [CrossRef]
5. National Environmental Policy Act (NEPA). *Environmental Impact Assessment (EIA) in the United States*; National Environmental Policy Act (NEPA): Washington, DC, USA, 1969.
6. Kamei, I.; Maruta, E. Study on Wind Environmental Problems Caused around Buildings in Japan. *J. Wind Eng. Ind. Aerodyn.* **1979**, *4*, 307–331. [CrossRef]
7. Yoshie, R.; Mochida, A.; Tominaga, Y.; Kataoka, H.; Harimoto, K.; Nozu, T.; Shirasawa, T. Cooperative Project for CFD Prediction of Pedestrian Wind Environment in the Architectural Institute of Japan. *J. Wind Eng. Ind. Aerodyn.* **2007**, *95*, 1551–1578. [CrossRef]

8. Leung, D.Y.C.; Yang, Y. Wind Energy Development and its environmental impact: A review. *Renew. Sustain. Energy Rev.* **2012**, *16*, 1031–1039. [CrossRef]
9. Steele, A. An Environmental Impact Assessment of the Proposal to build a Wind Farm at Langdon Common in the North Pennines, UK. *Environmentalist* **1991**, *11*, 195–212. [CrossRef]
10. Razak, A.A.; Hagishima, A.; Ikegaya, N.; Tanimoto, J. Analysis of air flow over building arrays for assessment of urban wind environ ment. *Build. Environ.* **2013**, *59*, 56–65. [CrossRef]
11. Kwon, Y.; Kim, J.; Kwon, S. Analyzing the Impact of Skyscraper wind in Coastal Areas. *J. Coast. Res.* **2021**, *114*, 266–270. [CrossRef]
12. Kheyari, P.; Dalui, S.K. Estimation of Wind Load on a Tall Building under Interference Effects: A Case Study. *Jordan J. Civ. Eng.* **2015**, *9*, 84–101.
13. Mou, B.; He, B.J.; Zhao, D.X.; Chau, K.W. Numerical Simulation of the effects of building dimensional variation on wind pressure distribution. *Eng. Appl. Comput. Fluid Mech.* **2017**, *11*, 293–309. [CrossRef]
14. Zheng, S.; Wang, Y.; Zhai, Z.; Xue, Y.; Duanmu, L. Characteristics of Wind Flow around a Target Building with Different Surrounding Building Layers predicted by CFD Simulation. *Build. Environ.* **2021**, *201*, 107962. [CrossRef]
15. Qiusheng, L.; Yuncheng, H.; Yinghou, H.; Kang, Z.; Xuliang, H. Monitoring wind effects of a landfall typhoon on a 600 m high skyscraper. *Struct. Infrastruct. Eng.* **2018**, *15*, 54–71.
16. Xiaoying, S.; Hao, L.; Ning, S.; Yue, W. Investigation on wind tunnel tests of the Kilometer skyscraper. *Eng. Struct.* **2017**, *148*, 340–356.
17. Xu-Liang, H.; Qiu-Shing, L.; Kang, Z.; Xiao, L. Comparative study between field measurements of wind pressures on a 600-m-high skyscraper during Super Typhoon Mangkhut and wind tunnel test. *Eng. Struct.* **2022**, *272*, 114958.
18. Korea Meteorological Admission. *Standard Specification for Automatic Weather Observation Equipment*; Korea Meteorological Admission: Seoul, Republic of Korea, 2018.
19. Tall Building Design Guidelines, City of Toronto, Canada. 2013. Available online: https://www.toronto.ca/city-government/planning-development/official-plan-guidelines/design-guidelines/tall-buildings/ (accessed on 8 May 2013).
20. Elton, H.; Florian, N.; Ani, P. The Wind Flow Effects and High-rise Buildings in Urban Spatial Morphology. In Proceedings of the 1st International Forum on Architecture and Urbanism, Tirana, Albania, 14–16 December 2017.
21. Tamura, Y.; Shimada, K.; Hibi, K. Wind Response of a Tower (Typhoon Observation at the Nagasaki Huis Ten Bosch Domtoren). *J. Wind Eng. Ind. Aerodyn.* **1993**, *50*, 309–318. [CrossRef]
22. Ishizaki, H. Wind Profiles, Turbulence Intensities and Gust Factors for Design in Typhoon-prone Regions. *J. Wind Eng. Ind. Aerodyn.* **1983**, *13*, 55–66. [CrossRef]
23. *ASCE 7-10*; Minimum Design Loads for Buildings and Other Structures. American Society of Civil Engineers: Reston, VA, USA, 2010.
24. Ishizaki, H. *Wind-Resistant Engineering*; Asakura: Tokyo, Japan, 1977; p. 27.
25. Shuyang, C.; Yukio, T.; Naoshi, K.; Mamoru, S.; Ikuo, N.; Yutaka, M. Wind characteristics of a strong typhoon. *J. Wind Eng. Ind. Aerodyn.* **2009**, *97*, 11–21.